which should be cited to refer to this work.

Effect of combined addition of graphene oxide and citric acid on superconducting properties of MgB_2

Sudesh [a], S. Das [b], C. Bernhard [b], G.D. Varma [a,*]

[a] Department of Physics, Indian Institute of Technology Roorkee, Roorkee 247667, India
[b] Department of Physics and Fribourg Centre for Nanomaterials-FriMat, University of Fribourg, Chemin du Musee 3, CH-1700 Fribourg, Switzerland

In the present work, polycrystalline samples with compositions MgB_2 + 3wt% GO + x wt% $C_6H_8O_7$ (x = 0, 5 and 10) have been synthesized to study the effect of combined addition of graphene oxide (GO) and citric acid ($C_6H_8O_7$) on superconducting properties of MgB_2. X-ray diffraction studies show the formation of hexagonal crystal structure of MgB_2 with space group P6/mmm in all synthesized samples. We observe that the addition of GO in the sample improves the grain connectivity and consequently enhances the critical current density significantly with no substantial change in T_c. However for this sample, there is no significant improvement in H_{c2} and H_{irr}. With the combined addition of GO and citric acid, the $J_C(H)$, H_{c2} and H_{irr} are observed to improve substantially as compared to the pristine MgB_2 and GO added MgB_2 samples. For example J_C(10 K, 5 T) of sample x = 10 has improved by a factor of ~15 as compared to pure MgB_2 sample and by a factor of ~5.5 as compared to the x = 0 sample. Furthermore, $H_{c2}(0)$ for x = 10 sample has enhanced by 13 T as compared to pure MgB_2 while it has increased by ~10 T in comparison to x = 0 sample. Enhanced flux pinning has been observed with the combined addition of GO and citric acid.

1. Introduction

Superconductivity in MgB_2, a binary intermetallic compound, was discovered by Akimitsu's group in 2001 [1]. This simple compound has a high superconducting critical temperature (T_c) of ~40 K. Its low anisotropy, absence of weak links and low fabrication cost make this material promising over the conventional low T_c superconductors for various technological applications. However, the rapid drop of critical current density (J_C) under the application of magnetic field is disadvantageous for taking this material into many practical applications. An extensive research has been done in order to further enhance the superconducting properties of MgB_2, such as critical current density (J_C), upper critical field (H_{c2}) and irreversibility field (H_{irr}). The substitution of C at the B-site by using various forms of C-containing compounds, e.g. SiC [2,3], C [4–6], B_4C [7], carbohydrates [8,9] and some organic compounds [6,10–12], have been found to be very effective in improving H_{c2}. However, the chemical substitution in MgB_2 leads to reduction in critical temperature, T_c [13,14]. More recently, it has been reported that the J_C values have been improved significantly by adding graphene [15,16], reduced graphene oxide (rGO) [17] and graphene oxide (GO) [18] into MgB_2 without affecting T_c much. It is studied that the addition of graphene, rGO or GO lead to improved inter-grain connectivity in the samples and thus leading to better conduction and hence J_C. In the previous study by our group [18], it has been found that with the addition of GO into MgB_2, J_C improves significantly with no substantial change in T_c. However, only a marginal improvement in H_{c2} and H_{irr} was observed. This is possibly due to negligible amount of C substitution at the B-site and hence less lattice distortion and consequently lesser charge carrier scattering. This has been proved from the XRD data which shows no significant change in lattice parameters on GO addition. In our previous study [6], we have found significant improvement in H_{c2} of citric acid ($C_6H_8O_7$) added MgB_2. In the present work, we have added GO and citric acid together in MgB_2 with the aim to improve $J_C(H)$, H_{c2} and H_{irr}. Polycrystalline samples with compositions MgB_2 + 3 wt% GO + x wt% $C_6H_8O_7$ (x = 0, 5 and 10) have been prepared using the standard solid-state reaction route. We observe that with the combined addition of GO and citric acid, the $J_C(H)$, H_{c2} and H_{irr} improve substantially as compared to the pristine MgB_2 and GO added MgB_2 samples. Enhanced flux pinning has been observed with the combined addition of GO and citric acid.

* Corresponding author at: Department of Physics, Indian Institute of Technology Roorkee, Roorkee 247667, Uttarakhand, India. Tel.: +91 1332 285353; fax: +91 1332 273560.
E-mail address: gdvarfph@iitr.ernet.in (G.D. Varma).

2. Experimental

All the bulk polycrystalline MgB_2 samples were synthesized by employing the standard solid-state reaction method. Graphene oxide (GO) used for the addition has been synthesized using the method developed by Marcano et al. [19] as explained earlier [18]. High quality Mg (Sigma Aldrich, 99.9% pure, ~100 μm grain size) and B (Sigma Aldrich, amorphous, 99%, submicron grains size) powders were weighed in appropriate quantities to form MgB_2. The mixture was properly ground and the resulting powder was pressed into rectangular pellets. We further synthesized the samples with compositions MgB_2 + 3 wt% GO + x wt% citric acid (x = 0, 5 and 10). For all samples, an extra 5 wt% quantity of Mg was added to compensate for the Mg loss during sintering. The pellets were put in a Fe-tube with holes in the cap (for the inlet of Ar/H_2 gas) for sintering. The samples were sintered at 850 °C in Ar/H_2 (9:1) for 3 h followed by quenching at 650 °C to room temperature. The samples are henceforth named as MB (MgB_2), MBG (MgB_2 + 3wt% GO), MBGC05 (MgB_2 + 3 wt% GO + 5 wt% citric acid) and MBGC10 (MgB_2 + 3 wt% GO + 10 wt% citric acid). The X-ray diffraction (XRD) pattern was recorded for phase identification of samples with a diffractometer (Bruker AXS, D8 ADVANCE) using Cu Kα radiation. The microstructure of all the samples was studied using field emission scanning electron microscope (FESEM). Resistivity measurements were carried out using standard four-probe technique under applied magnetic field up to 8 T. The DC magnetization measurements were done using the Vibrating Sample Magnetometer (VSM) facility of PPMS (Quantum Design) performed at University of Fribourg, Switzerland.

3. Results and discussion

The XRD patterns of MB, MBG, MBGC05 and MBGC10 samples are shown in Fig. 1. All the samples show MgB_2 main phase with trace amounts of MgO impurity phase. The indexing of characteristic peaks corresponding to MgB_2 is shown in Fig. 1. The peaks corresponding to MgO are marked by ∗. The presence of MgO is unavoidable with the present synthesis method due to some entrapped air before the sample is enclosed in the iron tube for sintering and also due to oxide nature of dopants. Refinement of the XRD patterns was done using X'pert HighScore to obtain the structural parameters such as lattice parameters, a and c and FWHM. The obtained parameters are listed in Table 1. The volume percentage of MgO as obtained from the refinement of the XRD data are shown in Table 1 for all samples. The inset in Fig. 1 shows the expanded view of peaks (110) and (002). It is clear, within the accuracy of measurements, that with increasing wt% of citric acid the shifting of (110) peak is more prominent than that of (002) peak, which indicates a significant change in the in-plane lattice parameters. We observe only a small change in the lattice parameters of MBG sample with respect to MB sample. However, when citric acid is added in the samples together with GO, a substantial change in the lattice parameters a and c with respect to MB sample is observed as listed in Table 1. From the variation of lattice parameters, the content of carbon entering into the lattice is calculated using the relation: $y = 7.5 \times \Delta c/a$, where $\Delta c/a$ is the change in c/a value as compared to that of the pure MgB_2 sample and y is the exact value of C (atomic wt%) substituted for B in the sample [13]. The obtained values (see Table 1) show that in case of GO addition, the amount of C entering into the lattice is very small, while in case of citric acid and GO addition, there is larger amount of C substituting for B into the lattice. This is possibly due to lack of dissociation of GO into its constituents at the sintering temperature, thus less carbon is available for doping.

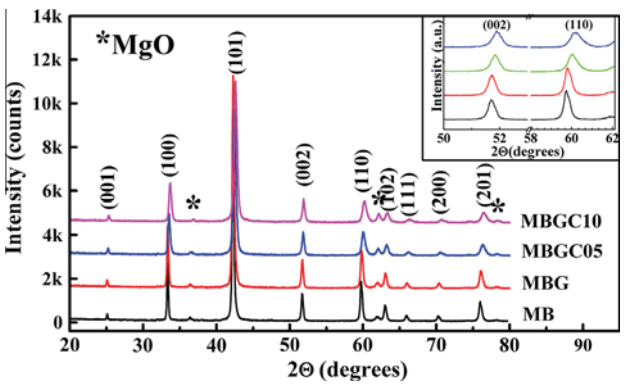

Fig. 1. X-ray diffraction patterns for MB, MBG, MBGC05 and MBGC10 samples. ∗ Represents the impurity phase MgO in all the samples.

The variation of full width at half maximum (FWHM) of all the samples obtained for the peaks (002) and (110) of MgB_2 are shown in Fig. 2. The FWHM represents the peak broadening in the sample and is influenced by crystallite size and lattice strain [20]. We observe from this figure that on addition of citric acid, the increase in FWHM of peak (110) is more than that of the peak (002). As the (110) plane corresponds to the in-plane lattice, so the broadening of (110) indicates increased distortion in the ab-plane due to C-substitution at the B-site of MBGC05 and MBGC10 samples. The lattice strain and crystallite size of the samples have been calculated using the Williamson-Hall [21] plots for all the samples. The calculated values for strain are shown in Fig. 2. It is observed that as compared to MB sample, the lattice strain has increased significantly in MBG, MBGC05 and MBGC10 samples. This further confirms the increased lattice distortion in MBG, MBGC05 and MBGC10 samples. The crystallite sizes for all the samples are given in Table 1. We see that the crystallite size of the samples has decreased with addition of citric acid.

FESEM micrographs of all the samples are presented in Fig. 3. We observe that the grain size has reduced with increased citric acid doping in the sample which confirms the XRD results of increased FWHM values. Also it is clearly observed from the micrographs that in the samples added with GO, grain connectivity is improved in comparison to the pure MgB_2 sample as is clear from the improved mass density (see Table 1). This feature has also been reported earlier for graphene, rGO and GO added samples [16], [17]. However, in the GO and citric acid added samples, connectivity is better than the pure MgB_2 sample but less than the GO added sample.

The temperature dependence of resistivity, normalized with its room temperature value ($\rho(T)/\rho(300\ K)$), of all the polycrystalline samples is shown in Fig. 4(a). Fig. 4(b) shows the superconducting transition in the temperature range 35–40 K. The critical temperatures (T_c), defined as the onset of superconducting transition, are listed in Table 2. The T_c is 38.84 K for pure MgB_2. For the GO added sample, we observe no significant change in T_c (=38.67 K). However, T_c decreases for the citric acid added samples, T_c = 38.20 K and 37.92 K for MBGC05 and MBGC10 samples, respectively. This is due to the increased substitution of C at the B-site in the lattice. The normal state resistivity ($\rho_{40\ K}$) for GO doped sample is almost the same as that of the pure MgB_2 sample while with combined addition of GO and citric acid $\rho_{40\ K}$ has increased, this is due to the enhanced impurity scattering with C substitution as well as the increased MgO content in the MBGC05 and MBGC10 samples. In polycrystalline samples, the grain connectivity is a major factor to affect the conduction in the material [22]. The porous nature of MgB_2 and the presence of MgO impurity phase tend to decrease the grain connectivity. The grain connectivity in MgB_2 can be estimated by knowing the value of $\Delta\rho$ ($\rho_{300\ K} - \rho_{40\ K}$) as suggested by Rowell [22]. From this parameter, the effective area cross

Table 1
Lattice parameters; a and c, actual quantity of doped C (y), MgO content, sample dimensions, mass density and crystallite size for all the samples.

Sample	a (Å)	c (Å)	y (%)	MgO (%)	Sample dimensions (mm^3)	Mass density (g/cm^3)	Crystallite size (nm)
MB	3.0859 (2)	3.5242 (1)	0	8.6	$3.6 \times 2.8 \times 3.2$	1.067	65.9
MBG	3.0822 (3)	3.5225 (2)	0.62	10.4	$4.38 \times 2.0 \times 2.44$	1.430	61.4
MBGC05	3.0777 (1)	3.5242 (2)	2.28	12.8	$4.80 \times 1.72 \times 1.81$	1.213	49.0
MBGC10	3.0775 (2)	3.5290 (2)	3.51	13.1	$4.75 \times 1.92 \times 2.55$	1.134	43.0

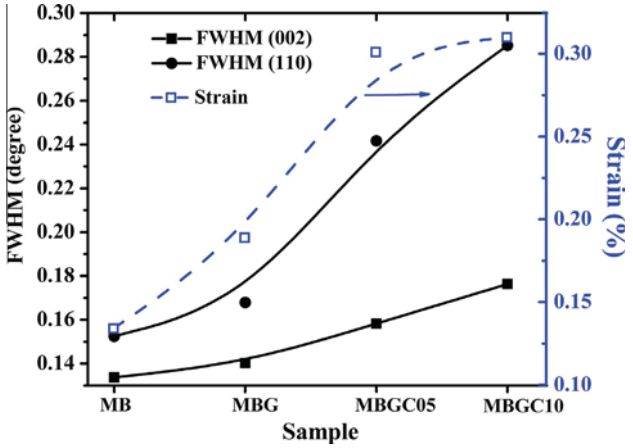

Fig. 2. Variation of full width at half maximum (FWHM) of (110) and (002) peaks and strain for all the samples.

section for current flow, A_f can be calculated using the formula: $A_f = \Delta\rho_{ideal}/\Delta\rho$, where $\Delta\rho_{ideal} = 7.3\ \mu\Omega$ cm, the value for a fully connected sample [22]. The calculated values of A_f are shown in Table 2. We observe that the A_f improves in MBG sample by a factor of ~2 as compared to the MB sample. The A_f values of MBGC05 and MBGC10 samples are also significantly larger than the pristine MgB_2 sample but has decreased as compared to the MBG sample. This is due to the increased amount of MgO content as well as increased C substitution which increases disorder in the GO and citric acid added samples. This result is in conformity with the FESEM results described above. The effect of increased MgO content is also evident from the decreased value of crystallite size of the samples (see Table 1). Disorder in a sample can be estimated by calculating the residual resistivity ratio ($RRR = \rho_{300\ K}/\rho_{40\ K}$). The calculated values of RRR for all the samples are listed in Table 2. From the table it is clear that the RRR values of GO and GO + citric acid added samples have decreased with respect to that of the pristine sample. Furthermore, RRR of MBGC05 and MBGC10 samples have smaller values as compared to that of MBG sample. The lowering of RRR values of MBG, MBGC05 and MBGC10 samples with respect to MB sample suggests increased disorder and hence increased impurity scattering in the GO and GO + citric acid added samples. Moreover, as compared to GO-added sample, in GO + citric acid added samples disorder and impurity scattering have enhanced. The increased disorder may be favorable to $J_C(H)$ behavior by increasing pinning as well as to H_{c2} in the sample. Fig. 4(c–f) shows the temperature variation of resistivity in applied magnetic field (0–8 T) near the transition region.

The upper critical field (H_{c2}) and irreversibility field (H_{irr}) are calculated by following the criteria $H_{c2} = H(\rho = 0.9\rho_{40\ K})$ and $H_{irr} = H(\rho = 0.1\rho_{40\ K})$, where $\rho_{40\ K}$ is the normal state resistivity or the

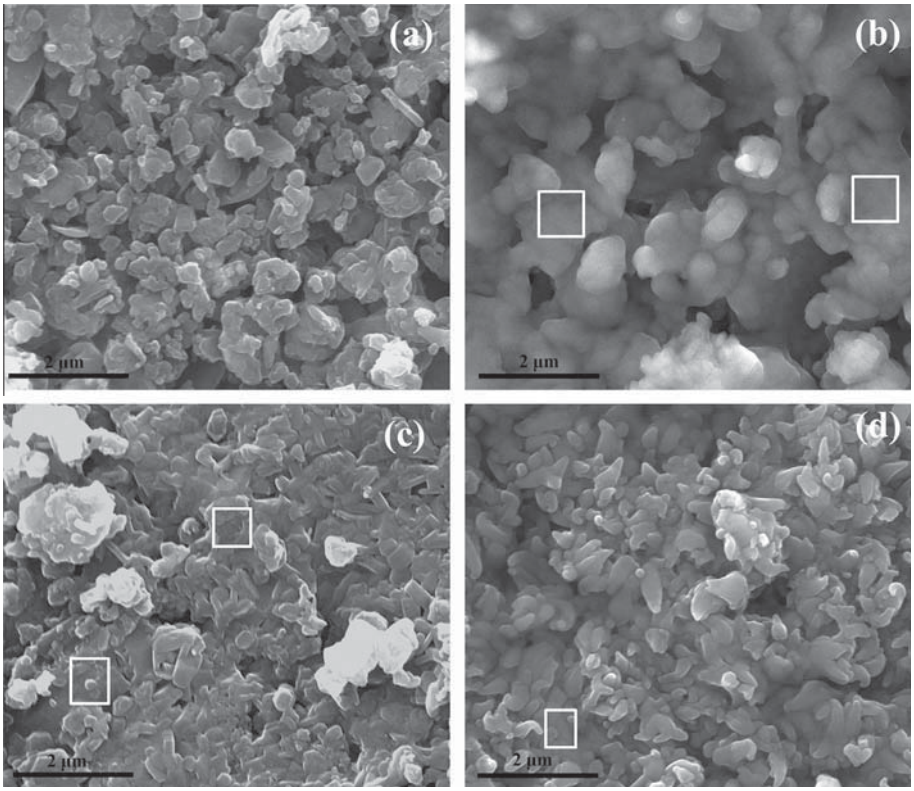

Fig. 3. FESEM micrographs for (a) MB, (b) MBG, (c) MBGC05 and (d) MBGC10 samples. Squares boxes in (b), (c) and (d) shows denser areas where grains seem well connected.

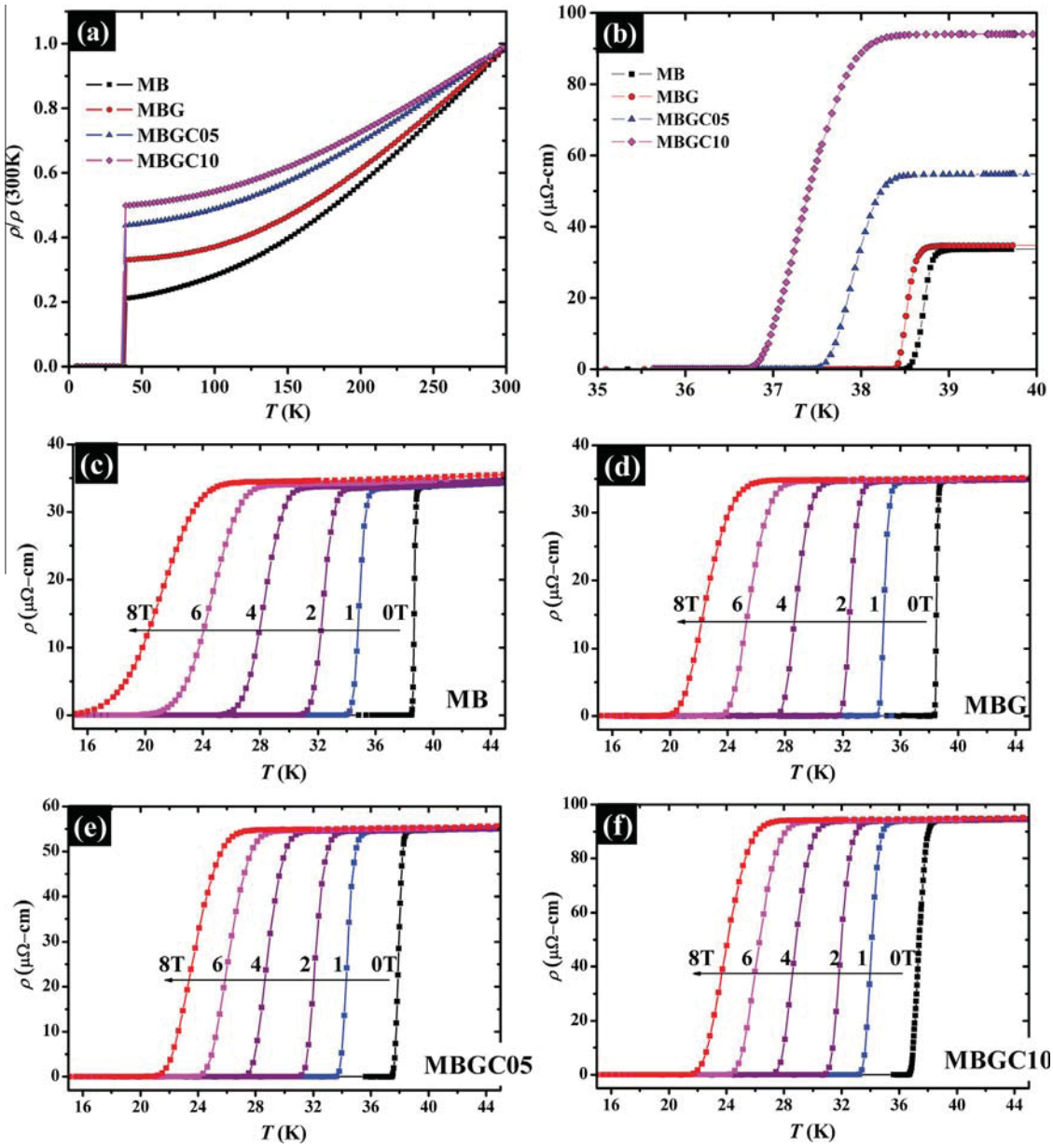

Fig. 4. (a) Normalized resistivity ($\rho/\rho(300\,K)$) vs temperature plots for all the samples. (b) Resistivity plots for all the samples in the transition region (35–40 K). Magnetoresistivity plots for the samples (c) MB, (d) MBG, (e) MBGC05 and (f) MBGC10.

Table 2
Critical temperature (T_c), Active area cross-section (A_f), residual resistivity ratio (*RRR*), upper critical fields calculated using Eq. (2) ($H_{c2}(0)$) and by using WHH model, Eq. (1) ($H_{c2}^{WHH}(0)$); and critical current density, J_C at 1 T and 5 T calculated at 10 K and 20 K.

Sample	T_c (K)	A_f (%)	RRR	$\mu_0 H_{c2}(0)$	$\mu_0 H_{c2}^{WHH}(0)$	J_C (A/cm^2)			
						10 K		20 K	
						1 T ($\times 10^5$)	5 T ($\times 10^3$)	1 T ($\times 10^4$)	5 T ($\times 10^2$)
MB	38.84	5.89	4.69	24.09	16.93	0.73	1.82	5.35	0.43
MBG	38.67	10.53	3.01	26.72	18.25	0.94	4.95	7.03	1.55
MBGC05	38.20	10.25	2.28	34.41	21.30	1.45	14.27	7.90	5.12
MBGC10	37.92	7.74	2.00	37.02	22.68	1.85	27.10	10.47	11.91

resistivity at 40 K. The variation of H_{c2} and H_{irr} with temperature for all the samples is shown in Fig. 5(a). We clearly see that the $H_{c2}(T)$ and $H_{irr}(T)$ behavior has improved substantially for the MBG, MBGC05 and MBGC10 samples over that of MB sample. Werthamer–Helfand–Hohenberg (WHH) model (see Eq. (1)) is most commonly employed to estimate the value of $H_{c2}(0)$, but this model underestimates the $H_{c2}(0)$ as discussed by Huang et al. [23]. So, we have also used the GL-theory for two-band superconductors to calculate the $H_{c2}(0)$ values. For the temperature dependence of H_{c2}, the GL-equation for a two-band superconductor [24,25] like MgB_2 is given by Eq. (2). However, in order to compare the results with previous studies, we have also calculated $H_{c2}(0)$ values using

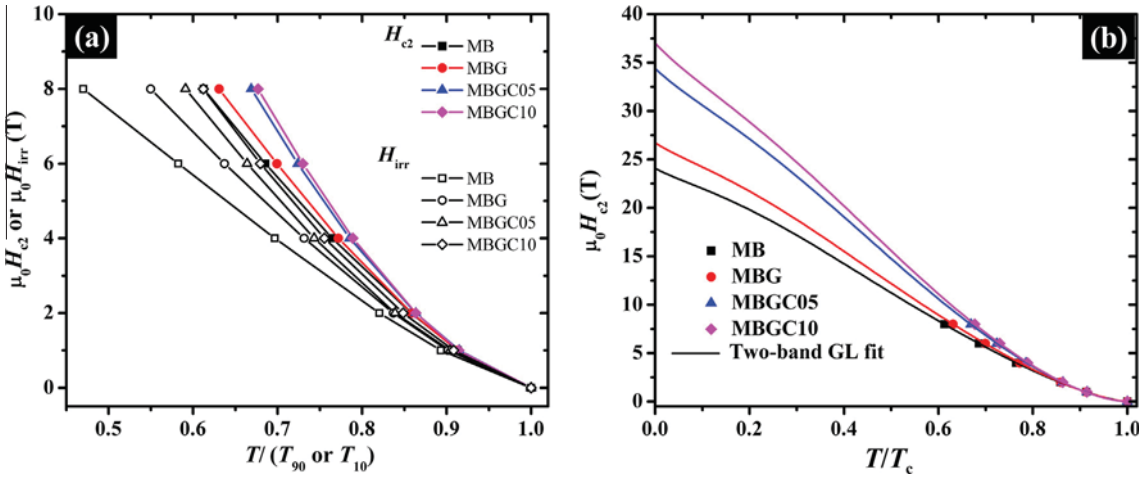

Fig. 5. (a) The $\mu_0 H_{c2}$ or $\mu_0 H_{irr}$ vs $T/(T_{90}$ or $T_{10})$ ($T_{90/10}$ is the temperature where the value of ρ is (0.9 or 0.1)ρ_n, ρ_n is the normal state resistivity) plots for MB, MBG, MBGC05 and MBGC10 samples. $\mu_0 H_{c2}$ is shown by solid symbols and $\mu_0 H_{irr}$ by open symbols. (b) The fitting of $\mu_0 H_{c2}(T)$ by two-band GL-theory (Eq. (2)).

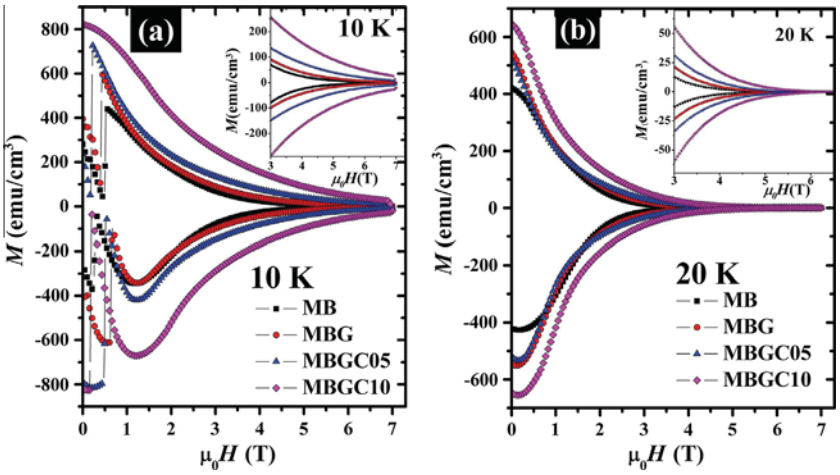

Fig. 6. Magnetic hysteresis loops (M–H) for all the samples at (a) 10 K and (b) 20 K. The insets show enlarged view at high magnetic fields.

WHH model, Eq. (1). The values of $H_{c2}(0)$ thus calculated are listed in Table 2. In Eq. (2), the value of α determines the temperature dependence of H_{c2}. l and m are fitting parameters. The negative curvature at low temperatures is accounted by the ratio l/m and it is assumed to be sensitive to the electronic structure. The temperature region which shows negative curvature is wide for $l > m$ and upper critical field shows linear temperature dependence for $l < m$. In fitting the $\mu_0 H_{c2}$ vs T data, we have used the values $l = 3$ and $m = -1$ [23]. The values of α obtained by fitting are 0.345, 0.391, 0.503 and 0.539 for MB, MBG, MBGC05 and MBGC10, respectively.

$$H_{c2}^{WHH}(T) = H_{c2}(0) T_c \left.\frac{dH_{c2}(T)}{dT}\right|_{T_c} \quad (1)$$

$$H_{c2}(T) = H_{c2}(0)\frac{\theta^{1+\alpha}}{1-(1+\alpha)\omega + l\omega^2 + m\omega^3},$$
$$\theta = T/T_c \text{ and } \omega = (1-\theta)\theta^{1+\alpha} \quad (2)$$

The data fitted with Eq. (2) are shown in Fig. 5(b). The fitted curves are shown by solid lines and the experimental data are shown by symbols. From the fitting, the obtained $H_{c2}(0)$ values of all samples are listed in Table 2. From the table we see that the GO and citric acid doped samples have higher $H_{c2}(0)$ values than the pure MgB_2 sample. The highest $H_{c2}(0)$ is obtained for MBGC10 sample ($H_{c2}(0) = 37$ T using Eq. (1), $H_{c2}^{WHH}(0) = 22.68$ T) which is comparable to the highest reported values [25–27] for polycrystalline MgB_2 samples. This result confirms that the addition of citric acid in combination with GO improves $H_{c2}(0)$ values substantially,

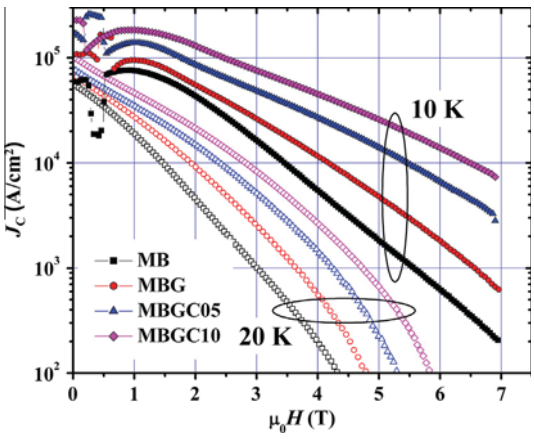

Fig. 7. Magnetic field dependent critical current density, J_C, at 10 K and 20 K.

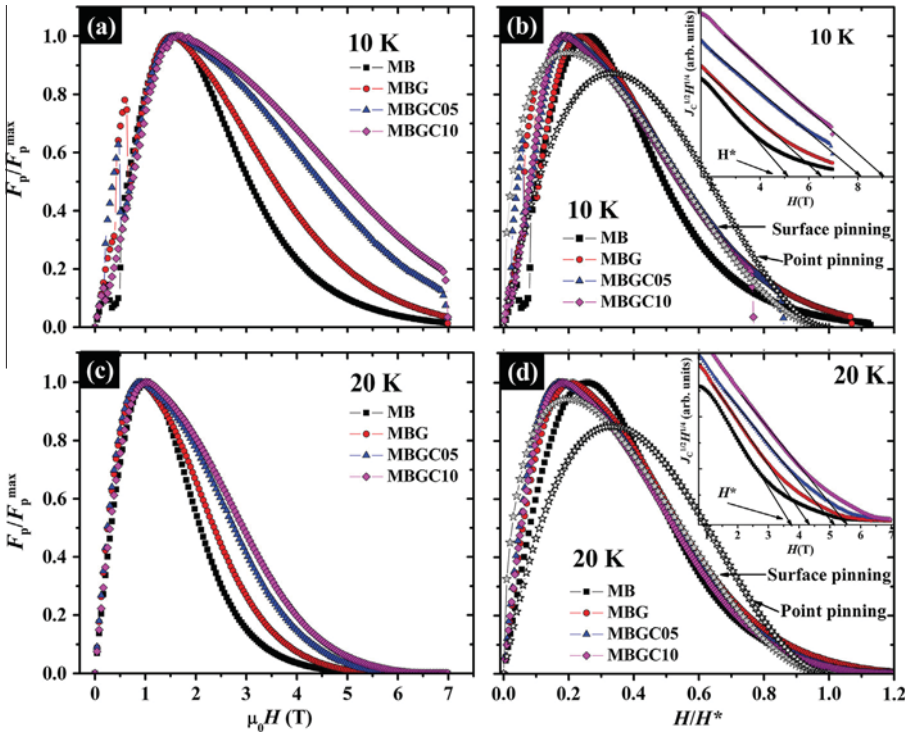

Fig. 8. Normalized flux pinning force density, F_p/F_p^{max} as a function of $\mu_0 H$ at 10 K (a) and at 20 K (c). (b) and (d) show the experimental data plotted as a function of H/H^*, H^* is the value of irreversibility field, calculated from the Kramer plot (shown in the insets). The theoretical curves corresponding to normal point pinning (PP) and surface pinning (SP) mechanisms are also shown in (b) and (d).

with only ~1 K decrease in T_c. The negative curvature near $T = 0$ obtained from GL-theory is unexpected. There is another model, known as Gurevich model [28–30], which accounts for the real situation for the effect of both bands on critical parameters. Furthermore, the improvement in H_{irr} of GO and citric acid added MgB_2 samples clearly suggests the enhanced pinning in the samples.

The magnetization measurements are done in the field range 0–7 T at 10 K and 20 K for all the samples as shown in Fig. 6(a) and (b), respectively. The increased loop width with the combined addition of GO and citric acid clearly indicates enhanced grain connectivity and improved pinning at high fields. The magnetic field dependence of J_C for all the samples is calculated from the magnetic hysteresis loops measured at 10 K and 20 K using the modified Bean formula $J_C(H) = 20\Delta M/(Va(1 - a/3b))$ A/cm^2, where ΔM is the width (in emu) of the magnetization loop, a and b are the dimensions (in cm) of the samples perpendicular to the direction of applied magnetic field and $a < b$ [31]. The $J_C(H)$ behavior of all the samples is shown in Fig. 7 at 10 K and 20 K. At 10 K, as shown in Fig. 7, flux jumps are observed in low field region of $J_C(H)$ behavior which is mainly caused by very low heat capacity and relatively high J_C values in MgB_2 [32]. The J_C value at 20 K and 1 T applied magnetic field for MBGC10 is 10.47×10^5 A/cm^2 which is almost twice that of MB sample. The highest J_C at 10 K and 5 T is observed for MBGC10 sample ($\sim 27.10 \times 10^4$ A/cm^2) which is ~15 times higher than the pristine MB sample. The $J_C(H)$ results obtained in the present study are comparable to the earlier reported results [26] for the best $J_C(H)$ behavior with only ~1 K decrease in T_c. The improvement in $J_C(H)$ behavior in the GO and citric acid added samples is possibly due to combined effect of improved grain connectivity and enhanced pinning in the samples. The enhanced pinning in the samples is also reflected in the H_{irr} behavior of GO and citric acid added samples.

Flux pinning force densities, $F_p = J_C \times H$, for all the samples are calculated from the magnetic critical current densities. The normalized pinning force density, F_p/F_p^{max} (F_p^{max} is the peak value of F_p for a given curve), as a function of applied field is shown in Fig. 8(a) and (c) for 10 K and 20 K, respectively. It is clearly observed that the strength of pinning force has increased quite significantly at higher fields. In order to study the nature of pinning mechanisms in all the samples, the normalized pinning force ($f_p = F_p/F_p^{max}$) is plotted as a function of $h = H/H^*$ (see Fig. 8(b) and (d) for 10 K and 20 K, respectively). Here, H^* is the value of irreversibility field calculated using Kramer plot: $J_C^{1/2}H^{1/4}$ vs (shown in the insets of Fig. 8(b) and (d) for 10 K and 20 K, respectively) [33]. In order to find out the possible pinning mechanism in all the samples, the plots are compared with the proposed theoretical model by Dew-Hughes [34] which gives a general scaling function $f_p \propto h^p(1 - h)^q$ to find out the possible pinning mechanism. Here, p and q are shape parameters depending on the type of dominant pinning mechanism present in the samples; $(p,q) = (1/2,2)$ indicates surface pinning and $(p,q) = (1,2)$ indicates normal point pinning as proposed by Kramer [35]. The theoretical curves corresponding to normal point pinning (PP) and surface pinning (SP) are shown in Fig. 8(b) and (d). On comparing the experimental data with the theoretical curves, we observe that the experimental curves do not follow the behavior of theoretical curves defining point pinning and surface pinning. Hence it is difficult to infer the dominant pinning mechanism present in the samples using this scaling behavior.

4. Conclusion

In summary, the systematic study of the effect of combined addition of GO and citric acid on the superconducting properties of MgB_2 has been carried out. It has been observed that with the addition of GO in the MgB_2 sample, the grain connectivity and thus J_C values have improved considerably while H_{c2} and H_{irr} improved marginally. On the other hand, the combined addition of GO and citric acid in the sample has led to a substantial improvement in $H_{c2}(0)$, H_{irr} and $J_C(H)$ behavior. The highest values of J_C and $H_{c2}(0)$

have been obtained for the sample with 3 wt% GO and 10 wt% citric acid addition (i.e. for MBGC10 sample). For this sample ~15-fold improvement in J_C(10 K, 5 T) over the pure MgB_2 sample and $H_{c2}(0)$ ~37 T (calculated using two-band GL-theory fit to the experimental data) have been observed. Thus, from the present investigation we observe that the superconducting properties ($J_C(H)$, H_{c2} and H_{irr}) of MgB_2 could be enhanced substantially by addition of GO in combination with a carbon dopant (e.g. carbohydrate in the present case).

Acknowledgments

The authors are thankful to Dr. Rajeev Rawat, UGC-DAE CSR, Indore centre for helpful discussions and carrying out the field dependent resistivity measurements. Sudesh thanks Ministry of Human Resources and Development (MHRD, Govt. of India), for providing the financial support. S Das and C Bernhard acknowledge funding by the Swiss National Science Foundation (SNF) Grant No. 200020-140225 and by Project No. 122935 of the Indo-Swiss Joint Research Program (ISJRP).

References

[1] J. Nagamatsu, N. Nakagawa, T. Muranaka, Y. Zenitani, J. Akimitsu, Superconductivity at 39 K in magnesium diboride, Nature 410 (2001) 63–64, http://dx.doi.org/10.1038/35065039.
[2] S.X. Dou, S. Soltanian, J. Horvat, X.L. Wang, S.H. Zhou, M. Ionescu, H.K. Liu, P. Munroe, M. Tomsic, Enhancement of the critical current density and flux pinning of MgB_2 superconductor by nanoparticle SiC doping, Appl. Phys. Lett. 81 (2002) 3419, http://dx.doi.org/10.1063/1.1517398.
[3] A. Matsumoto, H. Kumakura, H. Kitaguchi, B.J. Senkowicz, M.C. Jewell, E.E. Hellstrom, Y. Zhu, P.M. Voyles, D.C. Larbalestier, Evaluation of connectivity, flux pinning, and upper critical field contributions to the critical current density of bulk pure and SiC-alloyed MgB_2, Appl. Phys. Lett. 89 (2006) 132508, http://dx.doi.org/10.1063/1.2357027.
[4] M. Paranthaman, J.R. Thompson, D.K. Christen, Effect of carbon-doping in bulk superconducting, Physica C 355 (2001) 1–5.
[5] W.K. Yeoh, J.H. Kim, J. Horvat, X. Xu, M.J. Qin, S.X. Dou, Control of nano carbon substitution for enhancing the critical current density in MgB_2, Supercond. Sci. Technol. 19 (2006) 596–599, http://dx.doi.org/10.1088/0953-2048/19/6/030.
[6] N. Ojha, V.K. Malik, R. Singla, C. Bernhard, G.D. Varma, The effect of citric and oxalic acid doping on the superconducting properties of MgB_2, Supercond. Sci. Technol. 22 (2009) 125014, http://dx.doi.org/10.1088/0953-2048/22/12/125014.
[7] A. Yamamoto, J. Shimoyama, S. Ueda, I. Iwayama, S. Horii, K. Kishio, Effects of B_4C doping on critical current properties of MgB_2 superconductor, Supercond. Sci. Technol. 18 (2005) 1323–1328, http://dx.doi.org/10.1088/0953-2048/18/10/012.
[8] Y. Yang, C.H. Cheng, L. Wang, H.H. Sun, Y. Zhao, Effect of sorbic acid doping on flux pinning in bulk MgB_2 with the percolation model, Physica C 470 (2010) 1100–1102, http://dx.doi.org/10.1016/j.physc.2010.05.046.
[9] N. Ojha, V.K. Malik, R. Singla, C. Bernhard, G.D. Varma, The effect of carbon and rare earth oxide co-doping on the structural and superconducting properties of MgB_2, Supercond. Sci. Technol. 23 (2010) 045005, http://dx.doi.org/10.1088/0953-2048/23/4/045005.
[10] Q. Cai, Y. Liu, Z. Ma, D.A. Cardwell, Fishtail effects and improved critical current density in polycrystalline bulk MgB_2 containing carbon nanotubes, Physica C 492 (2013) 6–10, http://dx.doi.org/10.1016/j.physc.2013.05.002.
[11] W.X. Li, Y. Li, M.Y. Zhu, R.H. Chen, X. Xu, W.K. Yeoh, J.H. Kim, S.X. Dou, Benzoic acid doping to enhance electromagnetic properties of MgB_2 superconductors, IEEE Trans. Appl. Supercond. 17 (2007) 2778–2781.
[12] A. Vajpayee, V.P.S. Awana, G.L. Bhalla, P.A. Bhobe, A.K. Nigam, H. Kishan, Superconducting properties of adipic-acid-doped bulk MgB_2 superconductor, Supercond. Sci. Technol. 22 (2009) 015016, http://dx.doi.org/10.1088/0953-2048/22/1/015016.
[13] M. Avdeev, J.D. Jorgensen, R.A. Ribeiro, S.L. Bud'ko, P.C. Canfield, Crystal chemistry of carbon-substituted MgB2, Physica C 387 (2003) 301–306, http://dx.doi.org/10.1016/S0921-4534(03)00722-6.
[14] S. Lee, Recent advances in crystal growth of pure and chemically substituted MgB_2, Physica C 456 (2007) 14–21, http://dx.doi.org/10.1016/j.physc.2007.01.018.
[15] K.S.B. De Silva, X. Xu, S. Gambhir, X.L. Wang, W.X. Li, G.G. Wallace, S.X. Dou, Flux pinning mechanisms in graphene-doped MgB_2 superconductors, Scr. Mater. 65 (2011) 634–637, http://dx.doi.org/10.1016/j.scriptamat.2011.06.047.
[16] X. Xu, S.X. Dou, X.L. Wang, J.H. Kim, J.A. Stride, M. Choucair, W.K. Yeoh, R.K. Zheng, S.P. Ringer, Graphene doping to enhance the flux pinning and supercurrent carrying ability of a magnesium diboride superconductor, Supercond. Sci. Technol. 23 (2010) 085003, http://dx.doi.org/10.1088/0953-2048/23/8/085003.
[17] K.S.B. De Silva, S. Gambhir, X.L. Wang, X. Xu, W.X. Li, D.L. Officer, D. Wexler, G.G. Wallace, S.X. Dou, The effect of reduced graphene oxide addition on the superconductivity of MgB_2, J. Mater. Chem. 22 (2012) 13941, http://dx.doi.org/10.1039/c2jm30323j.
[18] Sudesh, N. Kumar, S. Das, C. Bernhard, G.D. Varma, Effect of graphene oxide doping on superconducting properties of bulk MgB_2, Supercond. Sci. Technol. 26 (2013) 095008, http://dx.doi.org/10.1088/0953-2048/26/9/095008.
[19] D.C. Marcano, D.V. Kosynkin, J.M. Berlin, A. Sinitskii, Z. Sun, A. Slesarev, L.B. Alemany, W. Lu, J.M. Tour, Improved synthesis of graphene oxide, ACS Nano 4 (2010) 4806–4814, http://dx.doi.org/10.1021/nn1006368.
[20] A. Serquis, Y.T. Zhu, E.J. Peterson, J.Y. Coulter, D.E. Peterson, F.M. Mueller, Effect of lattice strain and defects on the superconductivity of MgB_2, Appl. Phys. Lett. 79 (2001) 4399, http://dx.doi.org/10.1063/1.1428109.
[21] G.K. Williamson, W.H. Hall, X-ray line broadening from filed aluminium and wolfram, Acta Metall. 1 (1953) 22–31.
[22] J.M. Rowell, The widely variable resistivity of MgB_2 samples, Supercond. Sci. Technol. 16 (2003) R17–R27.
[23] X. Huang, W. Mickelson, B.C. Regan, A. Zettl, Enhancement of the upper critical field of MgB_2 by carbon-doping, Solid State Commun. 136 (2005) 278–282, http://dx.doi.org/10.1016/j.ssc.2005.08.003.
[24] I.N. Askerzade, A. Gencer, N. Guclu, On the Ginzburg–Landau analysis of the upper critical field H_{c2} in MgB_2, Supercond. Sci. Technol. 15 (2002) L13–L16.
[25] M. Mudgel, L.S.S. Chandra, V. Ganesan, G.L. Bhalla, H. Kishan, V.P.S. Awana, Enhanced critical parameters of nanocarbon doped MgB_2 superconductor, J. Appl. Phys. 106 (2009) 033904, http://dx.doi.org/10.1063/1.3186048.
[26] K.S.B. De Silva, X. Xu, X.L. Wang, D. Wexler, D. Attard, F. Xiang, S.X. Dou, A significant improvement in the superconducting properties of MgB_2 by co-doping with graphene and nano-SiC, Scr. Mater. 67 (2012) 802–805, http://dx.doi.org/10.1016/j.scriptamat.2012.07.014.
[27] C. Tarantini, H. Aebersold, V. Braccini, G. Celentano, C. Ferdeghini, V. Ferrando, et al., Effects of neutron irradiation on polycrystalline $Mg^{11}B_2$, Phys. Rev. B 73 (2006) 134518, http://dx.doi.org/10.1103/PhysRevB.73.134518.
[28] A. Gurevich, Enhancement of the upper critical field by nonmagnetic impurities in dirty two-gap superconductors, Phys. Rev. B 67 (2003) 184515, http://dx.doi.org/10.1103/PhysRevB.67.184515.
[29] A. Gurevich, S. Patnaik, V. Braccini, K.H. Kim, C. Mielke, X. Song, et al., Very high upper critical fields in MgB_2 produced by selective tuning of impurity scattering, Supercond. Sci. Technol. 17 (2004) 278–286, http://dx.doi.org/10.1088/0953-2048/17/2/008.
[30] A. Gurevich, Limits of the upper critical field in dirty two-gap superconductors, Physica C 456 (2007) 160–169, http://dx.doi.org/10.1016/j.physc.2007.01.008.
[31] C.P. Bean, Magnetization of high-field superconductors, Rev. Mod. Phys. 36 (1964) 31.
[32] I. Felner, V.P. Awana, M. Mudgel, H. Kishan, Avalanche of flux jumps in polycrystalline MgB_2 superconductor, J. Appl. Phys. 101 (2007) 09G101, http://dx.doi.org/10.1063/1.2669959.
[33] M. Eisterer, Calculation of the volume pinning force in MgB_2 superconductors, Phys. Rev. B 77 (2008) 144524, http://dx.doi.org/10.1103/PhysRevB.77.144524.
[34] D. Dew-Hughes, The critical current of superconductors: an historical review, Low Temp. Phys. 27 (2001) 713, http://dx.doi.org/10.1063/1.1401180.
[35] E.J. Kramer, Scaling laws for flux pinning in hard superconductors, J. Appl. Phys. 44 (1973) 1360, http://dx.doi.org/10.1063/1.1662353.